electronics

MDPI

Article

Phase-Noise Characterization in Stable Optical Frequency Transfer over Free Space and Fiber Link Testbeds †

Peter Barcik [1,*], Jan Hrabina [2], Martin Cizek [2], Zdenek Kolka [1], Petr Skryja [1], Lenka Pravdova [2], Ondrej Cip [2], Lucie Hudcova [1], Ondrej Havlis [3,4] and Josef Vojtech [3]

1 Department of Radioelectronics, Brno University of Technology, 616 00 Brno, Czech Republic; 164399@vut.cz (P.S.); hudcova@vut.cz (L.H.)
2 Department of Coherence Optics, Institute of Scientific Instruments of the Czech Academy of Sciences, 612 64 Brno, Czech Republic; lpravdova@isibrno.cz (L.P.)
3 Department of Optical Networks, CESNET z.s.p.o, 160 00 Prague, Czech Republic; ondrej.havlis@cesnet.cz (O.H.); josef.vojtech@cesnet.cz (J.V.)
4 Department of Telecommunications, Brno University of Technology, 616 00 Brno, Czech Republic
* Correspondence: barcik@vut.cz
† This paper is an extended version of our paper published at the 2022 International Conference on Broadband Communications for Next-Generation Networks and Multimedia Applications (CoBCom) under the title "Stable Optical Frequency Transmission over a Free-Space Optical Testbed", Graz, Austria, 12–14 July 2022.

Abstract: Time and frequency metrology depends on stable oscillators in both radio-frequency and optical domains. With the increased complexity of the highly precise oscillators also came the demand for delivering the oscillators' harmonic signals between delocalized sites for comparison, aggregation, or other purposes. Besides the traditional optical fiber networks, free-space optical links present an alternative tool for disseminating stable sources' output. We present a pilot experiment of phase-coherent optical frequency transfer using a free-space optical link testbed. The experiment performed on a 30 m long link demonstrates the phase-noise parameters in a free-space optical channel under atmospheric turbulence conditions, and it studies the impact of active MEMS mirror stabilization of the received optical wave positioning on the resulting transfer's performance. Our results indicate that a well-configured MEMS mirror beam stabilization significantly enhances fractional frequency stability, achieving the−14th-order level for integration times over 30 s.

Keywords: time and frequency metrology; optical frequency transfer; free-space optics; optical fiber link; phase noise; MEMS mirror

check for updates

Citation: Barcik, P.; Hrabina, J.; Cizek, M.; Kolka, Z.; Skryja, P.; Pravdova, L.; Cip, O.; Hudcova, L.; Havlis, O.; Vojtech, J. Phase-Noise Characterization in Stable Optical Frequency Transfer over Free Space and Fiber Link Testbeds. *Electronics* **2023**, *12*, 4870. https://doi.org/10.3390/electronics12234870

Academic Editors: Erich Leitgeb, Andrej Kos, Mariusz Głąbowski, Maciej Sobieraj, Hristo Danchov Ivanov, Wilfried Gappmair, Franz Teschl and Reinhard Teschl

Received: 31 October 2023
Revised: 26 November 2023
Accepted: 1 December 2023
Published: 2 December 2023

1. Introduction

Fundamental time and frequency metrology relies on highly stable oscillators, which operate in either the radio-frequency spectrum (ranging from MHz to GHz) [1,2] or the optical frequency spectrum (typical range in hundreds of THz). The highest stability in the radio-frequency region is attained by Cs atomic fountain clocks that achieve relative frequency stability up to 10^{-16} [3–5]. In the optical domain, the top performers currently are highly coherent lasers stabilized to quantum transitions of motion-cooled ions or optical lattice clocks based on neutral atoms exhibiting relative stability up to 10^{-18} or even better [6–8].

Characterization of such stable frequency sources typically requires a mutual comparison of their generated signals; among the several techniques, the beat-note frequency and phase-noise measurements are the most prevalent. Such a characterization requires the signals from the sources to be delivered to a single measuring point. Generally, the physical transport of these devices is infeasible and often nearly impossible due to the complexity of these systems and the requirements of their specific operational conditions, with a singular exception of (the currently developed) optical clocks dedicated as transportable by design [9–11].

An alternative approach is to find a means of transport solely for the generated stable frequency instead of transporting the entire oscillator device. The most notable interest attracted (especially in conjunction with the upcoming redefinition of the SI second) is the area of stable frequency transfers using optical links [12–17], often referred to (together with analogical transfer of precise time) as the umbrella term photonic transfers.

Photonic transfers are essential for the mutual comparison of two or more delocalized stable frequency sources; nonetheless, the application potential is broader. Different sources with different parameters (e.g., degrees of stability) might be aggregated to form a synthetic source with the parameters crafted to suit a particular application—for example, a combination of a low noise source and a source with good long-term stability might form the synthetic source with the characteristics superior to either of the original.

Another role of photonic transfers, which appears very interesting for the future, is the distribution (dissemination) of stable frequencies from highly stable sources to local stable generators. Such a role is crucial when precise frequency stability is needed for reliable device operation or detecting phenomena with high temporal resolution. These applications include gravity accelerometers monitoring Earth deformation for potential earthquakes, radio telescopes requiring precise synchronization to receive waves and correlate with other telescopes, and position detectors on artificial satellites.

Today, most photonic transfers use optical fibers that can transfer stable optical frequencies over hundreds or thousands of kilometers. The rise of information and communication technologies has facilitated the development of extensive optical networks that interconnected large cities and metropolitan areas with optical fibers. The methods for optical frequency multiplexing (for example, the dense wavelength-division multiplexing, DWDM) operated on these optical networks allow multiple optical signals (optical carriers) to be transmitted simultaneously over a single fiber. In such a framework, there are optical channels (communication streams based on a single optical carrier, also called lambdas in the technology jargon) that are not used for actual data transfer (called dark channels) than can be used for different applications, including the precise time and frequency transfers. The notable difference is in the requirements on the underlying infrastructure, as the dark channels dedicated to photonic transfers must be amplified by specialized bidirectional amplifiers with the same propagation path for both transmission directions [18]. Despite these increased demands, the existing fiber-optic infrastructure provides a feasible vehicle for the development of sizeable photonic transfer networks—a task that has already been addressed by several scientific consortiums at multinational scale [19,20].

Although fiber networks can and do serve well in many applications, they also exhibit certain drawbacks when used for photonic transfers. The optical path necessarily passes through a series of optical elements of various kinds, where each element causes different wavelengths to travel at different speeds (dispersion). The physical length of the optical fiber is affected by variations in environmental conditions, and this dynamic length change leads to traffic (phase) delays. Acoustic vibrations induce phase noise to transmit frequencies due to the Doppler effect. As a result, an optical fiber link is, in principle, an inherently unstable component of the transmission assembly: thorough characterization and potentially active stabilization of the fiber link's phase length is needed to ensure a reliable operation in delivering stable frequencies. Ongoing research is dedicated to developing new techniques that enhance the stability of disseminated frequency signals and mitigate these adverse effects. For example, the use of Hollow Core Fiber (HCF) has emerged as a promising solution to reduce thermal sensitivity and chromatic dispersion, which is problematic in the standard Single-Mode Fiber (SMF) [21]. Besides these drawbacks, there are also scenarios where suitable fiber-optic infrastructure is unavailable (for instance, when a communication endpoint is not connected to the Earth's surface), and using an alternative technology is inevitable.

One of the promising approaches (also strongly related to this paper) is a free-space optical transfer using the free-space optical links (FSO). FSO communication employs optical beams propagating in the atmosphere or outer space instead of optical fiber, so it is feasible when using optical cables is impractical or cost-ineffective and when traditional radio connections cannot meet the requirement for very high transmission speeds. However, the environmental influences are even more pronounced, and the performance of FSO systems can suffer from atmospheric turbulence, scattering, and attenuation and, consequently, a higher amount of environment-induced phase noise and even signal dropouts. The scientific efforts in this field are essentially and inseparably associated with techniques to mitigate unwanted atmospheric influences [22]. The principal aim is to study the properties of the atmosphere as a transmission channel and simultaneously examine the possibilities of adaptive optics for eliminating short-term and long-term signal outages.

Advanced FSO systems implement various beam control and tracking methods to reduce signal disruptions caused by the unstable atmospheric transmission medium [23,24]. Synchronization of the two optical timescales connected via a quadcopter-mounted retroreflector is presented in [25]. According to [26], combining optical time transfer and optical clocks presents the possibility of large-scale free-space networks that connect ground-based and future space-based optical clocks. In [27], authors present the concept of a high-precision Optical Atomic Clock (OAC) operating on an Earth-orbiting space station, which is being compared to more stable terrestrial OACs. The possibility of an optical-based satellite–ground link is investigated in [28].

Researchers have successfully demonstrated long-distance terrestrial FSO dissemination of optical clock and frequency [29,30]. In [31], frequency comb-to-comb stabilization made through a 1.3 km FSO link by coherent transfer is presented. An FSO system built on an outdoor 1.4 km path demonstrated the ability to transmit optical frequencies by employing fast beam tracking [32]. Additionally, phase-stabilized optical frequency transfer was successfully demonstrated over a 265 m horizontal FSO link, utilizing active piezo mirrors to suppress beam wandering [33].

Another innovative approach utilized pseudo-random binary sequences and significantly improved the stability and robustness of optical frequency transfer in FSO links under turbulent conditions [34]. Even though the FSO is usually considered point-to-point technology, the authors in [35] report on the exciting concept of high-performance silica integrated two-dimensional lens-assisted beam-steering array allowing the point-to-multipoint free-space optical frequency transfer.

This paper presents an experimental transmission of stable optical frequency through an experimental FSO testbed. The main aim is to characterize the impact of atmospheric turbulence on the induced phase noise and analyze the (positive) influence of active stabilization of the received optical beam position using a Micro Electronic Mechanical System (MEMS) on the transfer. The phase-noise analysis of the precise frequency transfer supplements the results.

The work is a part of current research on the Czech national photonic network for precision time and frequency transfers [36], with the aim to extend the potential of precise time and frequency dissemination to locations outside the reach of optical fiber link infrastructure.

The following sections are structured as follows: Section 2 describes the experimental facility, including the experimental FSO testbed. Section 3 presents the measurement results and discusses the results; Section 4 concludes the paper.

2. The Experiment

The experimental FSO testbed follows our previous work [37], and it is used to evaluate transmission properties and induced phase noise during the stable optical frequency transfer. We conducted the experimental measurements on a 30 m FSO channel outdoors under the naturally occurring atmospheric turbulences. We carried out measurements with and without stabilization of the laser beam spot position by MEMS mirror and for different settings of the PID regulator. The measurement setup is shown in Figure 1.

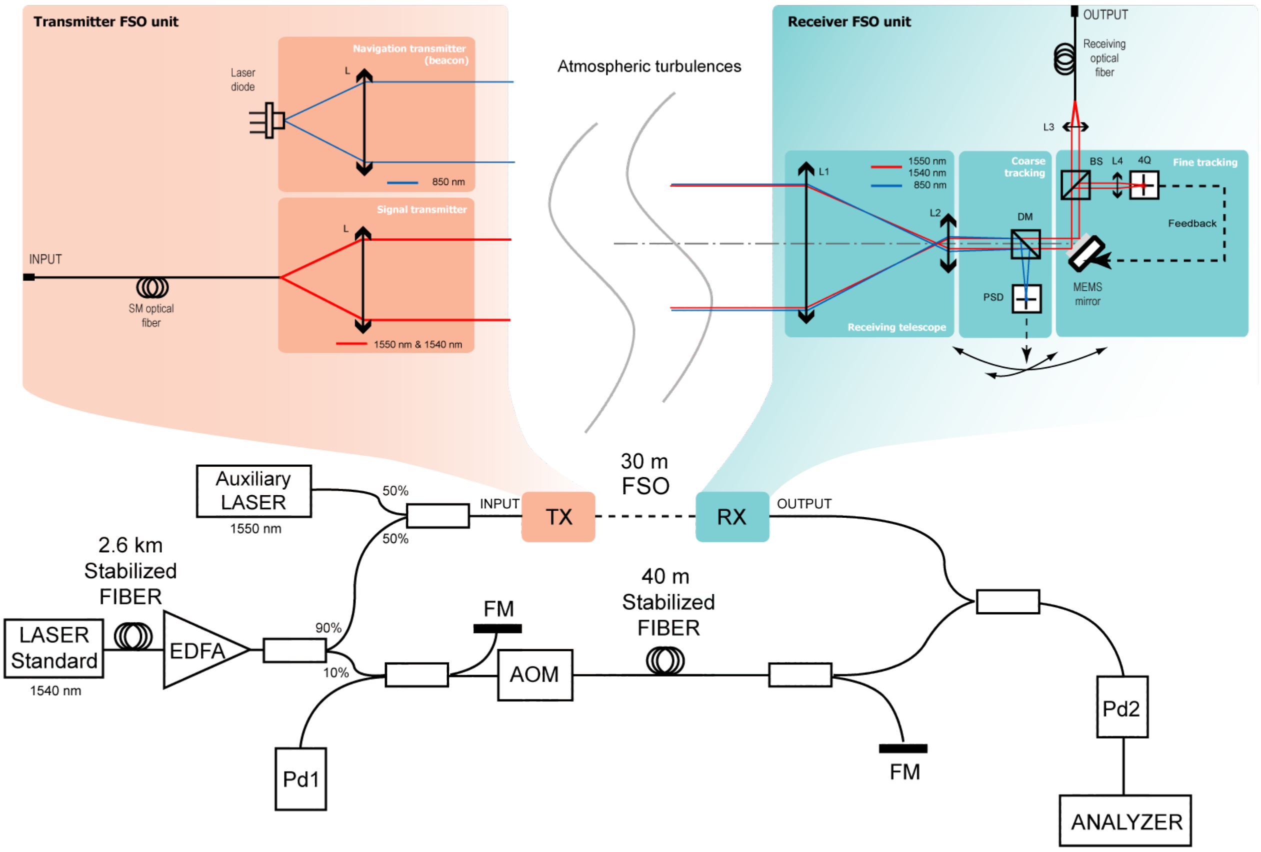

Figure 1. The schematic of the experiment: EDFA—Erbium-doped fiber amplifier, AOM—Acousto-optic modulator, Pd1, Pd2—Photodetectors, TX—FSO transmitter, RX—FSO receiver, FM—Faraday mirror, PSD—position-sensitive detector, 4Q—four-quadrant photodiode, DM—dichroic mirror, BS—beam splitter, SM—single-mode optical fiber.

The 1540 nm laser standard, an Erbium-doped fiber laser locked to an ultra-stable optical cavity with a resulting linewidth of approximately 3 Hz, was located at the Institute of Scientific Instruments, Czech Academy of Sciences. The laser beam was delivered to the experiment site with a 2.6 km long phase-stabilized urban optical fiber link. At the experiment location, the laser signal was amplified by an EDFA amplifier to the level of 8 dBm, and the output of the EDFA was split into two paths with a ratio of 10:90. The first path comprises a 40 m phase-compensated optical fiber (referred to as 40 m fiber). The second path is a 30 m unidirectional FSO link. The fiber link served as the reference arm for the FSO link phase-noise measurement. The fiber link noise was actively compensated for by detuning the AOM (acousto-optic modulator) driving signal frequency in a closed loop. The fiber noise detection was based on a commonly used scheme built around an unbalanced Michelson interferometer formed of two fiber branches terminated by Faraday rotator mirrors (FM). The instantaneous phase deviation of the RF in-loop beat note registered by the photodetector Pd1 then served as the error signal. The resulting fiber noise suppression bandwidth is approx. 30 kHz. Besides the active fiber noise suppression, the AOM provides an optical frequency shift of 80 MHz, which is necessary for detecting the beat note between the fiber and FSO paths by the Pd2 photodetector. The photo of the fiber link locking setup is depicted in Figure 2a. Suppose we neglect the noise introduced by the stabilized optical fiber link (which will be later demonstrated to have several orders of magnitude lower amplitude). In that case, the noise of the captured RF beat-note signal can be considered to be the noise introduced by the FSO path. A real-time RF spectrum analyzer was used to convert this beat-note signal from Pd2 photodetector to baseband in-phase (I) and quadrature (Q) signals. These signals contained complete information about the instantaneous phase and amplitude of the beat note. The I and Q signals were digitized and stored during the measurement for off-line processing. Equations (1) and (2) describe how in-phase (I) and quadrature (Q) baseband signal samples related to the instantaneous phase ϕ_n (relative to the reference local oscillator of the spectrum analyzer) and the instantaneous amplitude A_n of the RF signal.

$$\phi_n = \arctan 2(I_n, Q_n),\ \phi_n \in (-\pi, \pi\rangle, \tag{1}$$

$$A_n = \sqrt{I_n^2 + Q_n^2}. \tag{2}$$

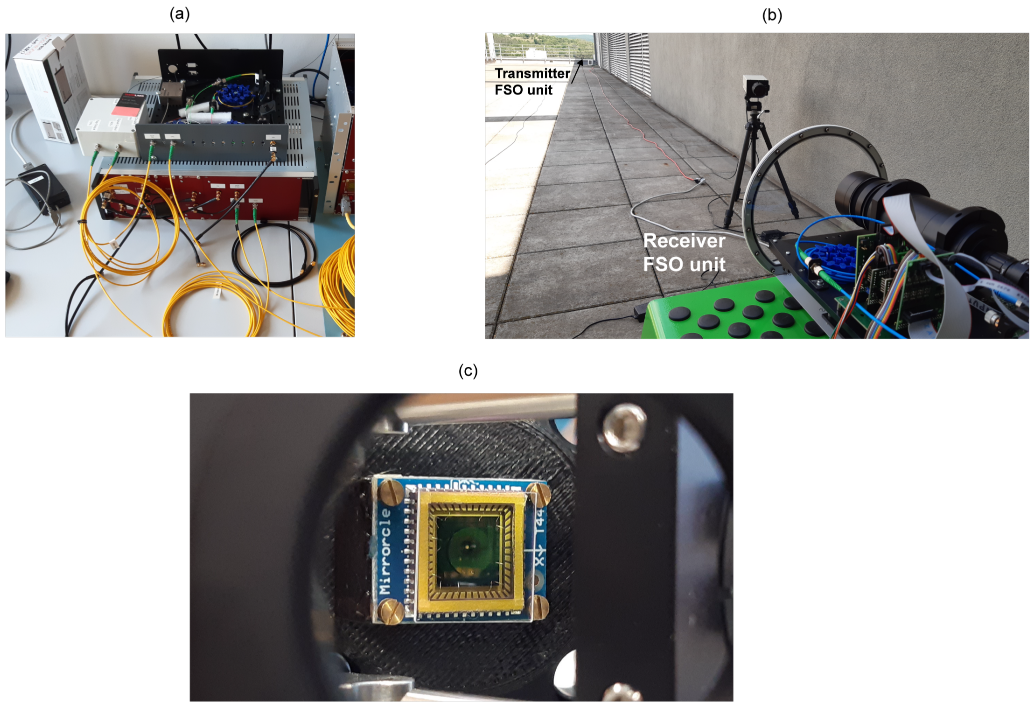

Figure 2. (**a**) Optical fiber stabilization units, (**b**) FSO testbed on the faculty roof, (**c**) Assembly details of the Mirrorcle MEMS.

To obtain a continuous phase signal, the instantaneous phase ϕ_n of the RF signal needs to be processed by an unwrapping algorithm to extend seamlessly its interval of possible values to $(-\infty, \infty)$. The resulting phase signal is then used for time and frequency-domain analysis, as described below.

The unidirectional FSO system comprises, as shown in the schematic in Figure 1 and photo of the testbed in Figure 2b, an optical fiber transmitter unit (TX) and an optical fiber receiver unit (RX). The transmitter unit took the carrier laser beam from the laser standard (at 1540 nm) fiber-coupled with an additional beam from an auxiliary laser (1550 nm), which was amplitude-modulated by a 20 kHz signal. The output from the single-mode transmitting fiber passes the collimating lens (L) and forms the output free-space beam. The divergence of this transmitted beam was set to 1 mrad. The second transmitter (used an 850 nm laser diode) served as a beacon to facilitate coarse alignment of the receiver side. This channel has a wider divergence to simplify the alignment procedure.

In the receiver unit, a refractive telescope receives both the beacon and signal optical waves. The optical waves are received by lens L1 with an aperture diameter of 76.2 mm and collimated by lens L2. The diameter of the laser beam behind the collimating lens L2 is about 3 mm. The carrier and beacon optical waves reached the dichroic mirror DM, which deflected the beacon beam towards the position-sensitive photodiode PSD. A microprocessor digitized and processed the electrical signal received from the PSD and produced a correction signal used for coarse (approximate) tilting of the FSO receiving terminal with a set of stepper motors. The used concept allows automatic search of the defined area and automatic adjustment of the receiving terminal so that the optical axes of the transmitting and receiving unit are unified.

After the combined 1540 nm and 1550 nm beam passed the DM, the MEMS mirror reflected it towards the beam splitter BS. From there, part of the optical power was incident on the 4Q photodiode and part on the front of the receiving optical fiber. The servo-control-based fine tilting system used the slowly modulated signal from the auxiliary 1550 nm laser. The MEMS mirror A5L2.2-5000AU, manufactured by Mirrorcle Technologies Inc., with a diameter of 5 mm, allowed for tilting in the range of $\pm 1^{\circ}$ in the x and y-axis. According to frequency response, the resonant frequency of the MEMS mirror was 1309 Hz for the x-axis and 1306 Hz for the y-axis. The implementation of the MEMS mirror into the optomechanical system is depicted in Figure 2c. The MEMS mirror, controlled by the feedback signal from the 4Q photodiode, serves to fine-tune the 1540 nm optical wave to the core of the receiving optical fiber. The total link attenuation was around 7 dB, while the geometric loss was 1 dB, and the receiving fiber coupling loss was 3 dB. The rest of the attenuation was attributed to the BS and other optical elements along the optical path inside the receiver.

The unit for active stabilization of Doppler shifts in the optical fiber path, and beat-note measurement unit with a spectral analyzer and FSO testbed is shown in Figure 2a,b.

3. Results and Discussion

For fine tracking of the laser spot in the FSO receiver unit, an auxiliary laser with a wavelength of 1550 nm AM modulated by a 20 kHz harmonic signal is used to suppress background radiation. The signal from the 4Q detector was processed by an AC logarithmic amplifier and sampled by a microprocessor. Based on this signal, the position of the laser beam is calculated, and a feedback signal is generated and fed into the MEMS mirror driver. The performance and stability of the entire tracking subsystem depend significantly on the correct PID controller settings. Despite the relatively short FSO link distance, the effects of atmospheric turbulence and vibrations on received optical power are noticeable.

3.1. Laser Beam Stabilization Performance

During the experiment, it was cloudy, and there was a light breeze with an average speed of 3 m/s. Figure 3 displays the signal from the 4Q photodiode over time alongside the MEMS mirror position for the x and y-axis. MEMS stabilization was initiated at 28 s (indicated by the red vertical line). Figure 3a,b show the signal from the 4Q photodiode as well as the MEMS mirror position signal in time. It is apparent from Figure 3c that the MEMS tries to compensate for the movement of the laser beam and keep it in the center of the 4Q photodiode. Nevertheless, some residual laser beam movement after MEMS activation remains noticeable. This could be attributed to improper PID regulation settings or compensation limitations only for lower-order wavefront distortions. Further adjustments in the fine-tracking system are necessary to achieve even better stabilization results. Due to the narrow field of view of the receiver, a slight divergence of the transmitting laser, and a relatively short FSO link distance, the FSO testbed was very sensitive to mechanical vibrations caused by wind gusts.

3.2. Analysis of the RF Beat-Note Signal

As mentioned before (Section 2), the photodetector Pd2 detects the RF beat note between the optical signal transferred over the FSO link and the optical signal from the stabilized fiber link, which serves as a reference. In an ideal case, without any disturbances in the FSO channel, this beat note would be a harmonic signal with a frequency of 80 MHz. Any disturbance introduced by the FSO transfer will thus manifest itself as a combination of phase, frequency, or amplitude noise of the beat-note signal. For stable frequency dissemination, the most important is to investigate the phase noise and fractional frequency stability of the channel.

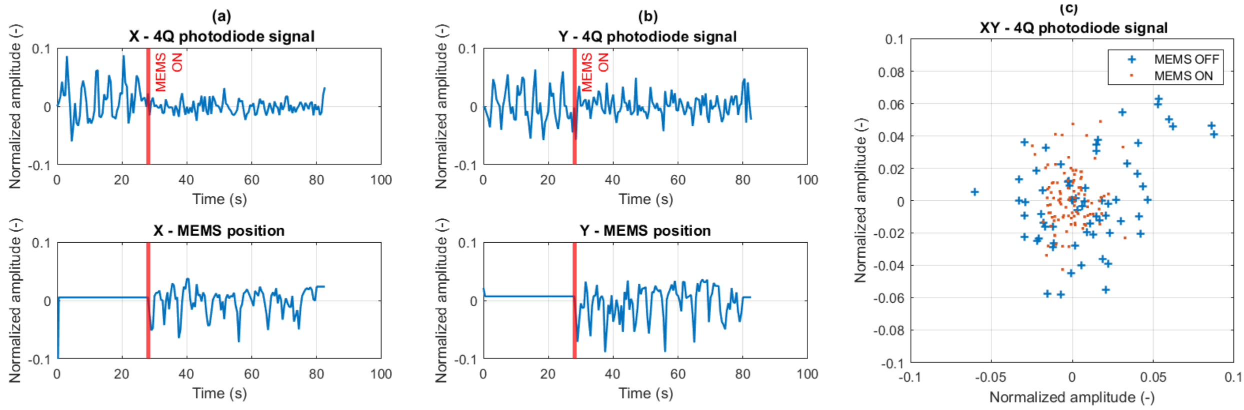

Figure 3. Signal from 4Q photodiode and MEMS mirror position in time for x-axis (**a**) and y-axis (**b**). The difference in the laser beam position with MEMS is ON and MEMS is OFF is displayed on the XY plot (**c**).

For four different scenarios, 5-min recordings of the RF beat note were acquired using a digital real-time RF spectrum analyzer. The instantaneous phase deviations of these recorded signals from the RF reference were computed using Equation (1). The phase deviation waveforms were investigated in the time domain and power spectral density representations. Finally, frequency deviations computed from the phase deviation signals were used to calculate overlapping Allan deviations to assess the fractional frequency stability of the FSO channel.

3.2.1. Time-Domain Analysis

The waveforms of phase deviations over time are shown in Figure 4. In the short-term perspective, where the DC component has been eliminated (a), it is apparent that active optical path stabilization, utilizing MEMS technology, significantly diminishes rapid phase excursions compared to a scenario lacking any stabilization. Over time, the cumulative impact of frequency offsets, frequency drifts, and signal dropouts caused by disturbances (leading to unpredictable outcomes) results in a continuous, long-term phase drift away from the zero value. In this way, the graphical representation in the long-term view (b) compares the overall robustness of all examined MEMS stabilization configurations. It is apparent that in the long-term, the phase deviation of the FSO channel with optimally configured stabilization stays close to zero mean value. At the same time, the other waveforms tend to drift to non-zero values.

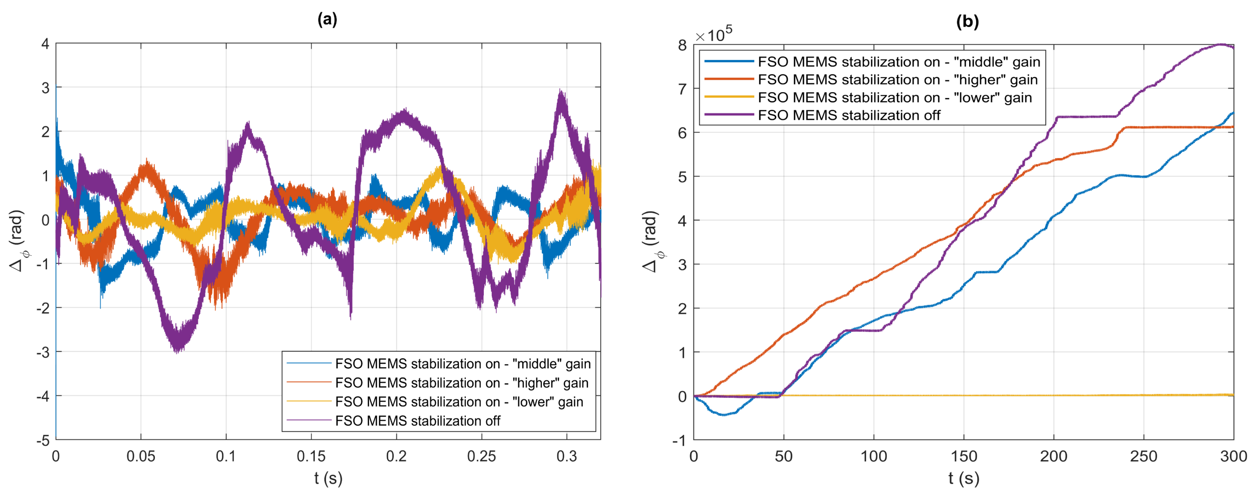

Figure 4. FSO vs. fiber link beat-note phase deviation in time: short-term comparison with linear drifts removed (**a**) and long-term comparison of raw phase data (**b**).

3.2.2. Frequency-Domain Analysis

The phase deviation signal was processed in the frequency domain to calculate the phase-noise power spectral density and the effective value of phase-noise contribution from the FSO transfer. To assess the fractional optical frequency stability of the FSO transfer, the phase deviation data were converted to frequency deviations and analyzed using overlapping Allan deviations.

The resulting phase-noise power spectral densities between the end of the fiber and free-space paths are plotted in Figure 5. From this figure, it is clear how the atmospheric turbulence increases phase noise on frequencies below 2 kHz. After activating MEMS stabilization, the phase noise is suppressed for frequencies below 100 Hz. However, there is a local maximum with a peak of around 1300 Hz, which is given by a resonance of the MEMS mirror. The height of this peak is dependent on the gain settings of the stabilization algorithm. To illustrate the measurement's noise floor, Figure 5 also includes plots depicting the power spectral densities of in-loop beat phase noise for both stabilized optical fiber links utilized in the experiment. This noise floor is several orders of magnitude lower than the actual measured phase noise induced by the FSO transfer.

Table 1 displays the effective values of phase noise in our measurements. These values agree with the investigation of phase-noise power spectral density. The integration interval was selected to encompass the frequencies to which the fiber links are most sensitive.

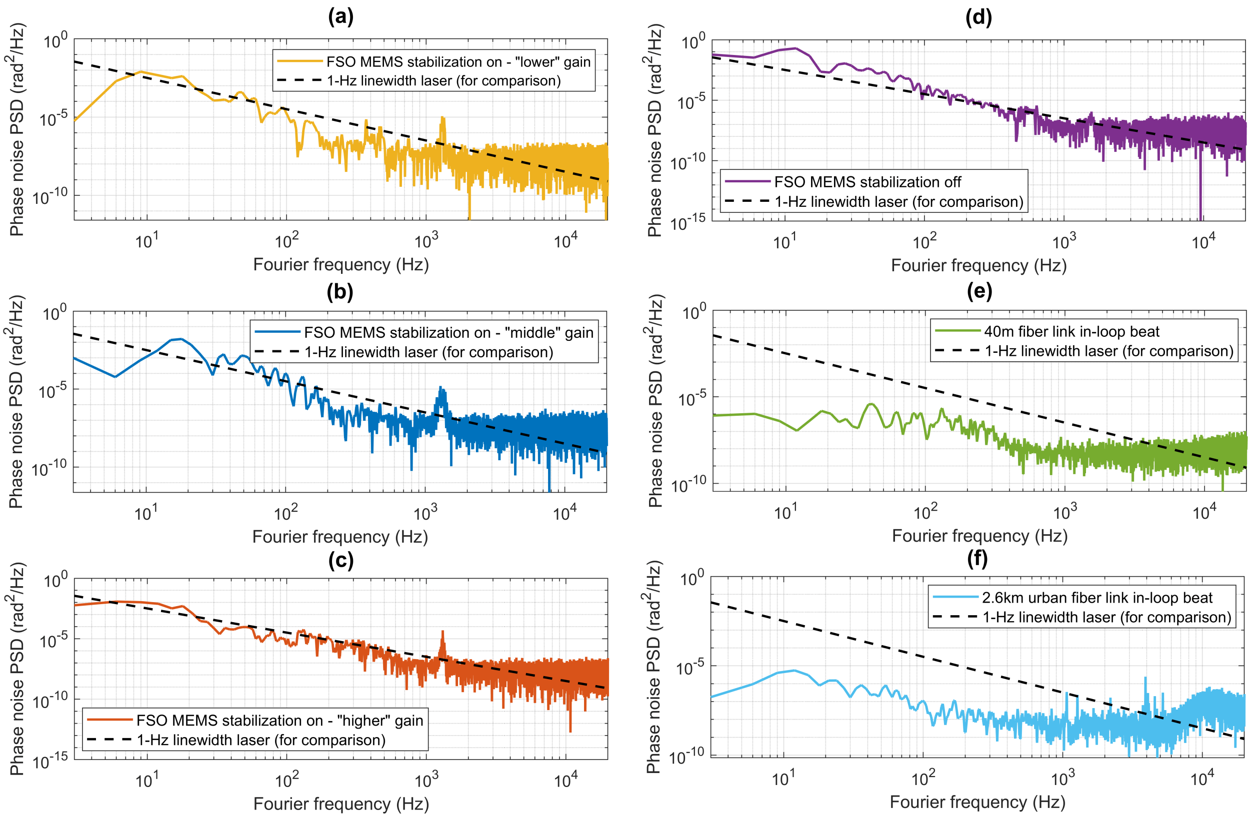

Figure 5. Phase-noise power spectral density: Different configurations of active FSO MEMS stabilization (**a**–**c**); FSO MEMS stabilization disabled (**d**); in-loop beat of the stabilized 40 m fiber link between FSO stations (**e**); in-loop beat of the stabilized 2.6 km urban fiber link (**f**). Model power spectral density of a 1 Hz FWHM laser is shown for comparison.

The instantaneous frequency deviations Δf of the acquired RF beat-note signal can be computed using the finite difference expressed by Equation (3) where ϕ is a discrete phase sample, T_S sampling period of the digitized signal and n index of the sample.

$$\Delta f_n = \frac{\phi_{n+1} - \phi_{n-1}}{4\pi \cdot T_S} \qquad \text{[Hz, rad, s]} \tag{3}$$

The fractional frequency stability, with respect to the optical frequency of the laser set at 194.734 THz, was determined from the acquired frequency samples. This calculation was performed using overlapping Allan deviations, as depicted in Figure 6. It is evident from the results that a properly configured beam stabilization significantly enhances the fractional frequency stability of the transmission by at least an order of magnitude. The relative stability of a free-running (or improperly configured) FSO transfer is constrained to the higher −13th order of magnitude. However, a properly optimized and stabilized FSO path can achieve fractional frequency stability levels as low as the −14th order of magnitude for integration times exceeding 30 s.

Table 1. Effective Values of Phase Noise.

Measurement Description	Integration Interval (Hz)	Phase Noise (rad)
Transmission in free space, MEMS stabilization on, "middle" gain, l = 30 m	1–4000	0.41
Transmission in free space, MEMS stabilization on, "higher" gain, l = 30 m	1–4000	0.38
Transmission in free space, MEMS stabilization on, "lower" gain, l = 30 m	1–4000	0.28
Transmission in free space, MEMS stabilization off, l = 30 m	1–4000	1.29
Fiber link in-loop beat (noise floor), l = 40 m	1–4000	0.01
Fiber link in-loop beat (noise floor), l = 2.6 km	1–4000	0.01

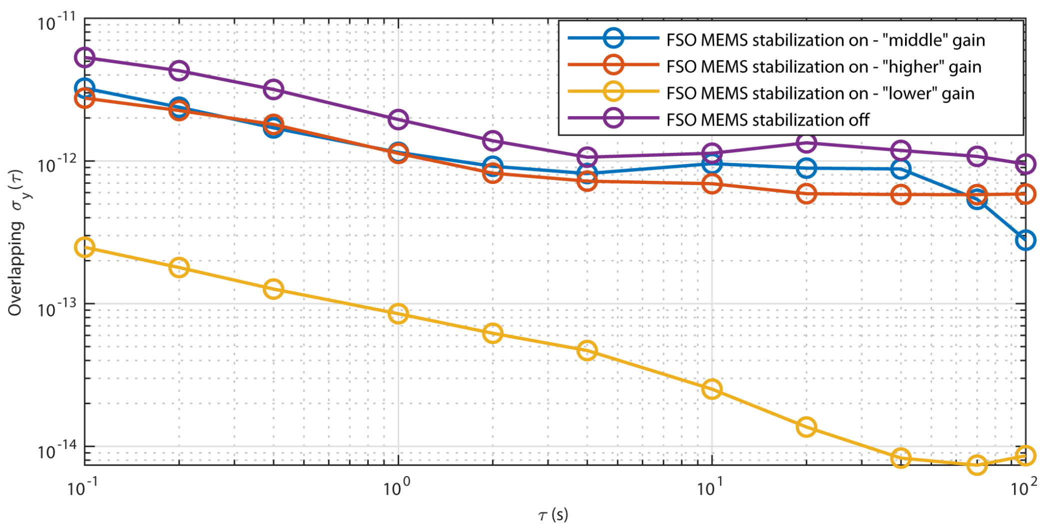

Figure 6. Fractional frequency stability of the FSO transfer relative to the working frequency of the laser.

4. Conclusions

This paper aimed to demonstrate and characterize the transmission of a continuous wave optical signal over a 30-m-long free-space optical link in the presence of atmospheric turbulences. Additionally, the study investigated the impact of active spatial stabilization using a MEMS mirror on the performance of the resulting transmission. Phase noise and intensity fluctuations of the received optical signal were analyzed with various configurations of the active beam stabilization settings. Although occasional signal disruptions occurred during the experiments due to atmospheric turbulence in the FSO transmission channel, we verified the feasibility of coherent, continuous wave transfer by actively adjusting the beam's position with a MEMS mirror and utilizing feedback from a four-quadrant detector. Appropriate PID controller settings significantly reduced phase noise caused by atmospheric turbulence. Subsequent work will focus on refining the fine-tracking algorithm to prevent signal disruptions and mitigate the resonance peak of the MEMS mirror. The bottleneck of the current FSO receiver is that we use a commercially available receiving lens that is not fully optimized for our needs. That is why we are currently working on the design of our custom lens, which will improve the coupling efficiency significantly. This is necessary for a longer FSO path with much greater demands on the power budget. An upcoming experiment will involve improved MEMS stabilization control, a redesign of the receiver's optics, and a longer FSO path.

Author Contributions: Conceptualization, P.B. and J.H.; data curation, P.B., L.H. and M.C.; funding acquisition, P.B., J.H. and O.C.; investigation, P.B., M.C. and J.H.; methodology, M.C.; resources, L.P., O.H. and J.V.; software, Z.K. and P.S.; supervision, Z.K. and O.C.; validation, P.B., J.H. and M.C.; visualization, P.B. and M.C.; writing—original draft preparation, P.B., J.H. and M.C. All authors have read and agreed to the published version of the manuscript.

Funding: This work has been supported by the FR CESNET (project FR710/2022), MEYS Czech Republic and ERDF (project CZ.02.1.01/0.0/0.0/16_026/0008460 "mQ-net"), Czech Academy of Sciences (project RVO:68081731) and the project 22IEM01 TOCK, which has received funding from the European Partnership on Metrology, co-financed from the European Union's Horizon Europe Research and Innovation Program and by the Participating States.

Data Availability Statement: Data are contained within the article.

Conflicts of Interest: The authors declare no conflict of interest.

Abbreviations

The following abbreviations are used in this manuscript:

MEMS	Micro Electronic Mechanical Systems
DWDM	Dense Wavelength-Division Multiplexing
HCF	Hollow Core Fiber
SMF	Single-Mode Fiber
FSO	Free-Space Optics
ISS	International Space Station
OAC	Optical Atomic Clock
AOM	Acousto-Optic Modulator
FM	Faraday Mirror
RF	Radio Frequency
EDFA	Erbium Dopped Fiber Amplifier
Pd	Photodetector
TX	Transmitter
RX	Receiver
PSD	Position-Sensitive Device
BS	Beam Splitter
DM	Dichroic Mirror
4Q	Four-Quadrant Photodetector

References

1. Ovchinnikov, Y.; Chalupczak, W.; Szymaniec, K.; Marra, G. Towards a high-stability Rb fountain frequency standard. In Proceedings of the 20th European Frequency and Time Forum, Braunschweig, Germany, 27–30 March 2006; pp. 186–188.
2. Bernier, L. Predictability of a Hydrogen Maser Time Scale. In Proceedings of the European Frequency and Time Forum, Besançon, France, 21–24 March 2005; pp. 438–441.
3. Meekhof, D.M.; Jefferts, S.R.; Stepanovíc, M.; Parker, T.E. Accuracy Evaluation of a Cesium Fountain Primary Frequency Standard at NIST. *IEEE Trans. Instrum. Meas.* **2001**, *50*, 507–509. [CrossRef]

4. Leo, P.J.; Julienne, P.S.; Mies, F.H.; Williams, C.J. Collisional Frequency Shifts in 133Cs Fountain Clocks. *Phys. Rev. Lett.* **2001**, *86*, 3743–3746. [CrossRef]
5. Parker, T.E. A Comparison of Cesium Fountain Primary Frequency Standards. In Proceedings of the EFTF, Toulouse, France, 22–25 April 2008; pp. 1–7.
6. Rosenband, T.; Hume, D.B.; Schmidt, P.O.; Chou, C.W.; Brusch, A.; Lorini, L.; Oskay, W.H.; Drullinger, R.E.; Fortier, T.M.; Stalnaker, J.E. Frequency Ratio of Al+ and Hg+ Single-Ion Optical Clocks; Metrology at the 17th Decimal Place. *Science* **2008**, *319*, 1808–1812. [CrossRef]
7. Gill, P.; Barwood, G.P.; Huang, G.; Klein, H.A.; Blythe, P.J.; Hosaka, K.; Thompson, R.C.; Webster, S.A.; Lea, S.N.; Margolis, H.S. Trapped Ion Optical Frequency Standards. *Phys. Scr.* **2004**, *T112*, 63–67. [CrossRef]
8. Ludlow, A.D.; Boyd, M.M.; Ye, J.; Peik, E.; Schmidt, P.O. Optical atomic clocks. *Rev. Mod. Phys.* **2015**, *87*, 637–701. [CrossRef]
9. Gellesch, M.; Jones, J.; Barron, R.; Singh, A.; Sun, Q.; Bongs, K.; Singh, Y. Transportable optical atomic clocks for use in out-of-the-lab environments. *Adv. Opt. Technol.* **2020**, *9*, 313–325. [CrossRef]
10. Takamoto, M.; Ushijima, I.; Ohmae, N.; Yahagi, T.; Kokado, K.; Shinkai, H.; Katori, H. Test of general relativity by a pair of transportable optical lattice clocks. *Nat. Photonics* **2020**, *14*, 411–415. [CrossRef]
11. Stuhler, J.; Abdel Hafiz, M.; Arar, B.; Bawamia, A.; Bergner, K.; Biethahn, M.; Brakhane, S.; Didier, A.; Fortágh, J.; Halder, M.; et al. Opticlock: Transportable and easy-to-operate optical single-ion clock. *Meas. Sens.* **2021**, *18*, 100264. [CrossRef]
12. Schioppo, M.; Kronjager, J.; Silva, A.; Ilieva, R.; Paterson, J.W.; Baynham, C.F.A.; Bowden, W.; Hill, I.R.; Hobson, R.; Vianello, A.; et al. Comparing ultrastable lasers at 7×10^{-17} fractional frequency instability through a 2220 km optical fibre network. *Nat. Commun.* **2022**, *13*, 212. [CrossRef]
13. Marra, G.; Margolis, H.S.; Lea, A.N.; Gill, P. High-stability microwave frequency transfer by propagation of an optical frequency comb over 50 km of optical fiber. *Opt. Lett.* **2010**, *37*, 1025. [CrossRef]
14. Marra, G.; Margolis, H.S.; Richardson, D.J. Dissemination of an optical frequency comb over fiber with 3×10^{-18} fractional accuracy. *Opt. Express* **2012**, *20*, 1175–1782. [CrossRef]
15. Grosche, G.; Terra, K.; Predehl, K.; Holzwarth, R.; Lipphardt, B.; Vogt, F.; Sterr, U.; Schnatz, H. Optical frequency transfer via 146 km fiber link with 10^{-19} relative accuracy. *Opt. Lett.* **2009**, *34*, 2270–2272. [CrossRef]
16. Hong, F.; Musha, M.; Takamoto, M.; Inaba, H.; Yanagimachi, S.; Takamizawa, A.; Watabe, K.; Ikegami, T.; Imae, M.; Fujii, Y.; et al. Measuring the frequency of s Sr optical lattice clock using a 120 km coherent optical transfer. *Opt. Lett.* **2009**, *34*, 5. [CrossRef]
17. Fujieda, M.; Kumagai, M.; Nagano, S.; Yamaguchi, A.; Hachisu, H.; Ido, T. All-optical link for direct comparison of distant optical clocks. *Opt. Express* **2011**, *19*, 16498–16507. [CrossRef]
18. Vojtech, J.; Slapak, M.; Skoda, P.; Radil, J.; Havlis, O.; Altmann, M.; Munster, P.; Velc, R.; Kundrat, J.; Altmannova, L.; et al. Joint accurate time and stable frequency distribution infrastructure sharing fiber footprint with research network. *Opt. Eng.* **2017**, *56*, 027101. [CrossRef]
19. Vojtěch, J.; Altmannová, L.; Smotlacha, V.; Velc, R.; Vohnout, R.; Schnatz, H.; Liebisch, T.C.; Capone, V.; Chiotis, T.; Roberts, G.; et al. CLONETS-DS—Clock Network Services-Design Study Strategy and innovation for clock services over optical-fibre networks in Europe. In Proceedings of the Conference on Lasers and Electro-Optics, San Jose, CA, USA, 9–14 May 2021; Optica Publishing Group: Washington, DC, USA, 2021; p. JTu3A.30.
20. Cantin, E.; Lopez, O.; Amy-Klein, A.; Chardonnet, C.; Cantin, E.; Tonnes, M.; Meynadier, F.; Pottie, P.E.; Quintin, N.; Camisard, E.; et al. REFIMEVE+: Optical Frequency Dissemination Over 2×1300 km of a Telecom Network. In Proceedings of the 2019 Joint Conference of the IEEE International Frequency Control Symposium and European Frequency and Time Forum (EFTF/IFC), Orlando, FL, USA, 14–18 April 2019; pp. 1–3. [CrossRef]
21. Feng, Z.; Marra, G.; Zhang, X.; Fokoua, E.R.; Sakr, H.; Hayes, J.R.; Poletti, F.; Richardson, D.J.; Slavík, R. Stable Optical Frequency Comb Distribution Enabled by Hollow-Core Fibers. *Laser Photonics Rev.* **2022**, *16*, 2200167. [CrossRef]
22. Sharma, D.; Tripathi, A.; Kumari, M. FSO systems for next generation networks: A review, techniques and challenges. *J. Opt. Commun.* **2022**. [CrossRef]
23. Mai, V.V.; Kim, H. Beam Control and Tracking Techniques for High- Altitude Airborne Free-Space Optical Communication Systems. In Proceedings of the 2020 International Topical Meeting on Microwave Photonics, MWP 2020, Virtual Conference, 24–26 November 2020; pp. 5–8. [CrossRef]
24. Singh, R.; Feng, F.; Hong, Y.; Faulkner, G.; Deshmukh, R.; Vercasson, G.; Bouchet, O.; Petropoulos, P.; O'Brien, D. Design and Characterisation of Terabit/s Capable Compact Localisation and Beam-Steering Terminals for Fiber-Wireless-Fiber Links. *J. Light. Technol.* **2020**, *38*, 6817–6826. [CrossRef]
25. Bergeron, H.; Sinclair, L.C.; Swann, W.C.; Khader, I.; Cossel, K.C.; Cermak, M.; Deschênes, J.D.; Newbury, N.R. Femtosecond time synchronization of optical clocks off of a flying quadcopter. *Nat. Commun.* **2019**, *10*, 1819. [CrossRef] [PubMed]
26. Caldwell, E.D.; Deschenes, J.D.; Ellis, J.; Swann, W.C.; Stuhl, B.K.; Bergeron, H.; Newbury, N.R.; Sinclair, L.C. Quantum-limited optical time transfer for future geosynchronous links. *Nature* **2023**, *618*, 721–726. [CrossRef]
27. Schkolnik, V.; Budker, D.; Fartmann, O.; Flambaum, V.; Hollberg, L.; Kalaydzhyan, T.; Kolkowitz, S.; Krutzik, M.; Ludlow, A.; Newbury, N.; et al. Optical atomic clock aboard an Earth-orbiting space station (OACESS): Enhancing searches for physics beyond the standard model in space. *Quantum Sci. Technol.* **2022**, *8*, 014003. [CrossRef]
28. Shen, Q.; Guan, J.Y.; Zeng, T.; Lu, Q.M.; Huang, L.; Cao, Y.; Chen, J.P.; Tao, T.Q.; Wu, J.C.; Hou, L.; et al. Experimental simulation of time and frequency transfer via an optical satellite–ground link at 10–18 instability. *Optica* **2021**, *8*, 471–476. [CrossRef]

29. Kang, H.J.; Yang, J.; Chun, B.J.; Jang, H.; Kim, B.S.; Kim, Y.J.; Kim, S.W. Free-space transfer of comb-rooted optical frequencies over an 18 km open-air link. *Nat. Commun.* **2019**, *10*, 4438. [CrossRef] [PubMed]
30. Shen, Q.; Guan, J.Y.; Ren, J.G.; Zeng, T.; Hou, L.; Li, M.; Cao, Y.; Han, J.J.; Lian, M.Z.; Chen, Y.W.; et al. Free-space dissemination of time and frequency with 10–19 instability over 113 km. *Nature* **2022**, *610*, 661–666. [CrossRef] [PubMed]
31. Yang, J.; IL Lee, D.; Shin, D.C.; Lee, J.; Kim, B.S.; Kang, H.J.; Kim, Y.J.; Kim, S.W. Frequency comb-to-comb stabilization over a 1.3-km free-space atmospheric optical link. *Light. Sci. Appl.* **2022**, *11*, 253. [CrossRef] [PubMed]
32. Yang, J.; Kang, H.J.; Lee, K.; Lee, J.; Kim, Y.J.; Kim, S.W. Phase-stabilized free-space link for optical frequency transfer. *Opt. Commun.* **2022**, *504*, 127481. [CrossRef]
33. Dix-Matthews, B.P.; Schediwy, S.W.; Gozzard, D.R.; Savalle, E.; Esnault, F.X.; Lévèque, T.; Gravestock, C.; D'Mello, D.; Karpathakis, S.; Tobar, M.; et al. Point-to-point stabilized optical frequency transfer with active optics. *Nat. Commun.* **2021**, *12*, 515. [CrossRef]
34. McSorley, S.; Gozzard, D.R.; Karpathakis, S.F.E.; Dix-Matthews, B.P.; Schediwy, S.W. Stabilized free space optical frequency transfer using digitally enhanced heterodyne interferometry. *Opt. Lett.* **2023**, *48*, 3637. [CrossRef]
35. Hu, L.; Xue, R.; Cao, X.; Liu, J.; Wu, K.; Wu, G.; Chen, J. Free-Space Point-to-Multiplepoint Optical Frequency Transfer With Lens Assisted Integrated Beam Steering. *IEEE Trans. Instrum. Meas.* **2022**, *71*, 515. [CrossRef]
36. Vojtech, J.; Smotlacha, V.; Havlis, O.; Vohnout, R.; Spacek, M.; Novak, T.; Andriantsarazo, E.; Slapak, M.; Altmannova, L.; Velc, R.; et al. National Infrastructure for Dissemination of Precise Time and Ultra-stable Optical Frequency also Aiming to Connect Quantum Sources—CITAF. In Proceedings of the Conference on Quantum Optics and Photon Counting, Prague, Czech Republic, 26–27 April 2023; SPIE: St Bellingham, WA, USA 2023; Volume 12570. [CrossRef]
37. Barcik, P.; Hrabina, J.; Cizek, M.; Skryja, P.; Kolka, Z.; Pravdova, L. Stable Optical Frequency Transmission over a Free Space Optical Testbed. In Proceedings of the 2022 International Conference on Broadband Communications for Next Generation Networks and Multimedia Applications (CoBCom), Graz, Austria, 12–14 July 2022; pp. 1–4. [CrossRef]